

Quantum-optimal-control-inspired ansätze for variational quantum algorithms

Alexandre Choquette,^{1,2} Agustin Di Paolo,¹ Panagiotis Kl. Barkoutsos,²

David Sénéchal,¹ Ivano Tavernelli,² and Alexandre Blais^{1,3}

¹*Institut quantique & Département de physique, Université de Sherbrooke, Sherbrooke J1K 2R1 QC, Canada*

²*IBM Quantum, Zurich Research Laboratory, Säumerstrasse 4, 8803 Rüschlikon, Switzerland*

³*Canadian Institute for Advanced Research, Toronto, ON, Canada*

(Dated: August 5, 2020)

A central component of variational quantum algorithms (VQA) is the state-preparation circuit, also known as ansatz or variational form. This circuit is most commonly designed to respect the symmetries of the problem Hamiltonian and, in this way, constrain the variational search to a subspace of interest. Here, we show that this approach is not always advantageous by introducing ansätze that incorporate symmetry-breaking unitaries. This class of ansätze, that we call Quantum-Optimal-Control-inspired Ansätze (QOCA), is inspired by the theory of quantum optimal control and leads to an improved convergence of VQAs for some important problems. Indeed, we benchmark QOCA against popular ansätze applied to the Fermi-Hubbard model at half-filling and show that our variational circuits can approximate the ground state of this model with significantly higher accuracy and for larger systems. We also show how QOCA can be used to find the ground state of the water molecule and compare the performance of our ansatz against other common choices used for chemistry problems. This work constitutes a first step towards the development of a more general class of symmetry-breaking ansätze with applications to physics and chemistry problems.

The rise of noisy intermediate-scale quantum processors [1, 2] requires us to find novel algorithms designed to attenuate the effects of noise. Variational quantum algorithms (VQA) are an example of such methods [3, 4]. These algorithms make use of a (noisy) quantum computer and a classical co-processor to minimize a cost function specified by a problem Hamiltonian \hat{H}_{prob} . This minimization is achieved by preparing a state that approximates the ground state of \hat{H}_{prob} on the quantum computer using an iterative procedure driven by the classical co-processor. Importantly, and thanks to the variational nature of these algorithms, this approach has been shown to potentially be resilient against noise, and well-suited to several applications including finance [5], pure mathematics [6], machine learning [7, 8], optimization problems [9, 10], quantum chemistry and materials [11–15], as well as quantum optics [16].

In VQAs, the state preparation requires the parameterization of a quantum circuit, referred to as the *ansatz* or *variational form*, that may or may not be structured around the problem. Recently, a considerable amount of effort has been invested in designing ansätze that preserve the symmetries of the problem Hamiltonian [17–22]. The goal of symmetry-preserving strategies is to constrain the variational search to a small vector space of interest, which in principle improves the probability of convergence to the target state with fewer optimizer iterations.

In this work, we highlight shortcomings of this approach. We then provide an ansatz that goes beyond symmetry-preserving methods by introducing a set of unitaries that break the symmetries of the problem Hamiltonian. To achieve this, we borrow ideas from the theory of quantum optimal control, where fast and high-fidelity operations are achieved through the addition of time-dependent symmetry-breaking terms to the

Hamiltonian. Focusing on fermionic systems, we incorporate such terms in a time-evolution-like ansatz [23] to obtain the Quantum-Optimal-Control-inspired Ansatz (QOCA). We benchmark this approach against common ansätze found in the literature for the Fermi-Hubbard model and apply these ideas to the water molecule with minimal modifications. We find that in most cases, this method produces approximations of the target ground state that are orders of magnitude more accurate. To understand this improvement, we show evidence that QOCA allows for an exploration in a slightly larger Hilbert space.

The paper is organized as follows: in Sect. I, we begin by presenting known approaches to the construction of the ansatz and then formally introduce QOCA and quantum optimal control theory in Sect. II. We also elaborate on our strategy for the selection of symmetry-breaking terms in Sect. II and explain how these can be incorporated into a variational ansatz for the Fermi-Hubbard model in Sect. III. Finally, we compare results obtained with the different approaches in Sect. IV.

I. VARIATIONAL ANSÄTZE

In the VQA framework, a quantum processor stores a quantum state $|\psi(\boldsymbol{\theta})\rangle$ parametrized by a collection of classical variational parameters $\boldsymbol{\theta}$. This state is prepared from a known and easily prepared reference state, $|\psi_0\rangle$, using a quantum circuit (the ansatz) $\hat{U}(\boldsymbol{\theta})$ such that $|\psi(\boldsymbol{\theta})\rangle = \hat{U}(\boldsymbol{\theta})|\psi_0\rangle$. The value of $\boldsymbol{\theta}$ is iteratively adjusted by a classical co-processor with the purpose of minimizing the cost function

$$E[\boldsymbol{\theta}] = \frac{\langle \psi(\boldsymbol{\theta}) | \hat{H}_{\text{prob}} | \psi(\boldsymbol{\theta}) \rangle}{\langle \psi(\boldsymbol{\theta}) | \psi(\boldsymbol{\theta}) \rangle}. \quad (1)$$

Numerous variational forms $\hat{U}(\boldsymbol{\theta})$ have been explored in the literature [18, 23–28]. Before introducing our approach, in this section we briefly review two widely used ansätze highlighting their advantages and disadvantages.

A. Hardware-efficient Ansatz

The Hardware-efficient Ansatz (HEA), introduced in Ref. [24], relies on gates that are native to the quantum hardware to produce circuits of high expressibility [29] and low depth. In particular, the HEA requires the application of successive blocks of parametrized single-qubit rotations followed by a generic entangling unitary $\hat{U}_{\text{Ent.}}$. An example for N qubits is

$$\hat{U}_{\text{HEA}}(\boldsymbol{\theta}) = \prod_d \hat{U}_{\text{Ent.}} \prod_{n=1}^N R_Z^{(n)}(\theta_{n,d}^Z) R_Y^{(n)}(\theta_{n,d}^Y), \quad (2)$$

where $\boldsymbol{\theta} = \{\theta_{n,d}^Z, \theta_{n,d}^Y\}$ collects all the variational parameters and $R_{\sigma_a}^{(n)}(\theta) = \exp[-i\theta\sigma_a/2]$ denotes a single-qubit rotation of angle θ around the $a \in \{x, y, z\}$ axis on qubit n . σ_a is the corresponding Pauli matrix. The parameter d is the number of layers, or *depth*, of the ansatz. Here and for the rest of this paper, we use the convention $\prod_i^N \hat{U}_i = \hat{U}_N \cdots \hat{U}_1$ for operator multiplication.

A feature of the HEA is that it is well suited to a broad exploration of the Hilbert space since it does not purposely favor a particular symmetry sector. This ansatz has already been experimentally implemented to prepare the ground state of small molecules [24], to simulate the folding of a few amino acid polymer [15], and to find the solution of classical optimization problems [10]. However, solving small instances of important problems does not provide a proof of scalability of the method for larger systems. Indeed, there is evidence that sufficiently random parametrized circuits, such as the ones produced by HEA, suffer from an exponentially vanishing gradient with the number of qubits making them more difficult to converge as the system size grows [30].

B. Variational Hamiltonian Ansatz

Ansätze that leverage the structure of the problem can avoid the aforementioned scalability issues since they do not explore the full exponentially large Hilbert space. Wecker *et al.* [23] introduced the Variational Hamiltonian Ansatz (VHA), which consists of a parametrized adaptation of the quantum circuit implementing time evolution under the problem Hamiltonian via Trotterization. In the VHA framework, the state-preparation unitary reads

$$\hat{U}_{\text{VHA}}(\boldsymbol{\theta}) = \prod_d \prod_j e^{i\theta_{j,d} \hat{H}_j}, \quad (3)$$

where $\boldsymbol{\theta} = \{\theta_{j,d}\}$ are the variational parameters and $\hat{H}_{\text{prob}} = \sum_j \hat{H}_j$ is the problem Hamiltonian expressed as the sum of non-commuting groups of terms

labeled \hat{H}_j . The depth d is associated with each time increment of the Trotterization of the time-evolution operator. If grouping the terms is done efficiently, this approach can be implemented using few variational parameters, therefore simplifying the classical optimization. However, depending on the complexity of the problem, circuits can be considerably longer as compared to those typically used with the HEA.

Fourier-transformed VHA (FT-VHA) To further reduce the number of variational parameters, it is possible to take advantage of the fact that most fermionic Hamiltonians can be written as $\hat{H}_{\text{prob}} = \hat{T} + \hat{V}$, where the diagonal bases of \hat{T} and \hat{V} are related through the fermionic Fourier transformation (FT) [31–33]. With the FT-VHA variational form, the FT is used to alternate between these bases at every Trotter step. In the context of quantum chemistry, this is known as the split-operator method [34, 35]. This idea was also recently introduced by Babbush *et al.* [36] for the variational quantum simulation of materials. The state-preparation unitary thereby reads

$$\begin{aligned} \hat{U}_{\text{FT-VHA}}(\boldsymbol{\tau}, \boldsymbol{\nu}) \\ = \prod_d \text{FT}^\dagger \left(\prod_j e^{i\tau_{j,d} \hat{T}_j} \right) \text{FT} \left(\prod_j e^{i\nu_{j,d} \hat{V}_j} \right), \end{aligned} \quad (4)$$

where $\boldsymbol{\tau} = \{\tau_{j,d}\}$ and $\boldsymbol{\nu} = \{\nu_{j,d}\}$ are the parameters associated with $\hat{T} = \sum_j \hat{T}_j = \text{FT} \hat{T} \text{FT}^\dagger$ and \hat{V} , respectively. Since now both \hat{T} and \hat{V} are diagonal, they only contain terms that commute and therefore the circuit decomposition of their exponentials can be achieved exactly, which was not the case of \hat{T} in the regular VHA. However, this comes at the cost of the long FT circuit [31, 33, 36].

Because they are built from the problem Hamiltonian, both VHA and FT-VHA respect the symmetries of the problem. For example, if no term of \hat{H}_{prob} allows the number of particles to change, this quantity will be conserved in the variational state $|\psi(\boldsymbol{\theta})\rangle$. This choice restricts the variational search to a relatively smaller subspace of the Hilbert space which, intuitively, can increase the performance of the VQA. Because of this, the VHA and FT-VHA ansätze are likely to perform better than HEA for large system sizes. However, as we show in Sect. IV, incorporating too much knowledge of the problem can also be detrimental.

Another popular approach in quantum chemistry is the UCCSD ansatz [3] which implements the exponential of a set of single- and double-excitation operators. Although not strictly Hamiltonian-based, this method preserves the parity symmetry of fermions and conserves the number of particles. Despite potentially providing accurate results, the UCCSD ansatz circuits can be very deep, limiting its applicability on near-term quantum devices.

II. QUANTUM-OPTIMAL-CONTROL-INSPIRED ANSATZ (QOCA)

To address the drawbacks of the ansätze discussed above, we propose an ansatz that borrows ideas from the theory of quantum optimal control [37–40], and which we therefore dub the Quantum-Optimal-Control-inspired Ansatz, or QOCA. The main idea behind QOCA resides in the introduction of carefully chosen symmetry-breaking unitaries into the symmetry-preserving ansatz VHA. In this section, we begin by reviewing some of the central aspects of the theory of quantum optimal control, and then show how these ideas can be incorporated in the design of variational forms.

A. Quantum optimal control

Quantum optimal control (QOC) theory describes the methods to optimally steer a quantum system from an initial state to a known final state [41]. Such techniques have been applied to a wide variety of problems including the quantum control of chemical reactions [42, 43], spins in nuclear magnetic resonance experiments [39, 44] and, more recently, to superconducting qubits [40, 45].

In this approach, the control Hamiltonian is specified by a set of time-independent drive Hamiltonians $\{\hat{H}_k\}$ whose amplitudes are parametrized by the time-dependent coefficients $\{c_k(t)\} \in \mathbb{R}$. The total Hamiltonian $\hat{H}(t)$ is then, in general, time-dependent such that

$$\hat{H}(t) = \hat{H}_0 + \sum_k c_k(t) \hat{H}_k, \quad (5)$$

with \hat{H}_0 the free, or drift, Hamiltonian of the controlled system. Solving the Schrödinger equation of the driven system results in the unitary $\hat{U}(t)$, which can propagate pure states through time as $|\psi(t)\rangle = \hat{U}(t)|\psi(0)\rangle$.

The system described by the Hamiltonian of Eq. (5), defined in a Hilbert space of dimension n , is said to be controllable if $\hat{U}(t)$ can be any matrix of $SU(n)$. In other words, the system is controllable if for any initial state $|\psi(0)\rangle$, there exists a set controls $\{c_k(t)\}$ and a time $T > 0$ for which the state $|\psi(T)\rangle$ can be any target state of the Hilbert space [41].

Quantum optimal control techniques, such as the GRAPE algorithm [39], provide a method for designing the control pulses $c_k(t)$ to achieve a desired state preparation. This is usually realized by seeking the set of controls and time T that optimize a cost function characterizing the state-preparation fidelity, which may include constraints such as the control time and the maximum pulse amplitudes.

In the GRAPE algorithm, time is discretized into N increments, or pixels, of duration Δt such that the total evolution occurs in a time $T = N\Delta t$. Using this

discretization, the continuous control fields $c_k(t)$ are now parametrized by the new constant piecewise control fields $\mathbf{u}_k = \{u_{k,j}\}$ as

$$c_k(t) = \sum_{j=0}^{N-1} u_{k,j} \Pi_j(t, \Delta t), \quad (6)$$

where $\Pi_j(t, \Delta t) \equiv \Theta(t - j\Delta t) - \Theta(t - (j+1)\Delta t)$ with Θ the Heaviside function. The time evolution operator for a time T therefore reads

$$\hat{U}(T) = \prod_{j=0}^{N-1} \exp \left[-i\Delta t \left(\hat{H}_0 + \sum_k u_{k,j} \hat{H}_k \right) \right], \quad (7)$$

and optimality is achieved by iteratively tuning the values of the discrete control fields $\{u_{k,j}\}$. Because this time propagator incorporates drive terms $\{\hat{H}_k\}$, that typically do not commute with the drift Hamiltonian, $\hat{U}(T)$ may implement unitary operations that are distinct from that generated by the drift Hamiltonian alone. In standard QOC problems, fast and efficient optimization of the control fields is possible because the target state (or operation) is known. This is, however, not the case in the context of VQA. Adapting these techniques to the VQA setting therefore requires to eliminate any information about the target state from the QOC cost function, therefore making the optimization less straightforward.

B. The QOCA variational form

Building on the concept of quantum optimal control, we modify the VHA by constructing a variational form which includes a set of *drive* terms $\{\hat{H}_k\}$ in addition to the problem Hamiltonian \hat{H}_{prob} . QOCA therefore mimics time evolution under the new Hamiltonian

$$\hat{H}_{\text{QOCA}}(t) = \hat{H}_{\text{prob}} + \sum_k c_k(t) \hat{H}_k, \quad (8)$$

where, by design, $[\hat{H}_{\text{prob}}, \hat{H}_k] \neq 0 \forall k$. We then construct the state-preparation circuit for QOCA by parameterizing the time-evolution-like operator

$$\hat{U}_{\text{QOCA}}(\boldsymbol{\theta}, \boldsymbol{\delta}) = \prod_d \left(\prod_j e^{i\theta_{j,d} \hat{H}_j} \prod_k e^{i\delta_{k,d} \hat{H}_k} \right), \quad (9)$$

where $\hat{H}_{\text{prob}} = \sum_j \hat{H}_j$ and $\boldsymbol{\theta} = \{\theta_{j,d}\}$ are the problem Hamiltonian parameters. Similar to Eq. (6), $\boldsymbol{\delta} = \{\delta_{k,d}\}$ are the discrete drive amplitudes of the control fields $c_k(t)$ of Eq. (8) which we use as variational parameters. Again, d is the depth of the ansatz and is analog to the steps in the time evolution.

A key concept of QOCA is that the problem Hamiltonian part helps constraining the variational search to the relevant symmetry sector of the Hilbert space, while

the *drive* part allows the ansatz to take shortcuts by temporarily exiting this sector. This concept is schematically drawn on Fig. 1b where we illustrate possible paths in the Hilbert space for the HEA, VHA and QOCA variational forms.

In principle, one has the freedom to select any drive Hamiltonians that do not commute with \hat{H}_{prob} . However, it is not straightforward to predict which choice will have the most positive impact on the outcome of the VQA. One option is to use an adaptive approach such as the one described in Refs. [46, 47]. However, in the next section we show how simple considerations can help to bound the number of interesting drive operators, and suggest which of these could be more effective.

C. Which drive Hamiltonians are useful for fermions?

With the objective of applying QOCA to the Fermi-Hubbard model, we consider the time-dependent fermionic Hamiltonian

$$\begin{aligned} \hat{H}_f(t) = & \sum_j (\alpha_j(t) \hat{a}_j + \alpha_j^*(t) \hat{a}_j^\dagger) \\ & + \sum_{i,j} \beta_{ij}(t) (\hat{a}_i^\dagger \hat{a}_j + \hat{a}_j^\dagger \hat{a}_i) + \sum_{i,j} \gamma_{ij}(t) \hat{a}_i^\dagger \hat{a}_i \hat{a}_j^\dagger \hat{a}_j, \end{aligned} \quad (10)$$

where \hat{a}_j^\dagger and \hat{a}_j are fermionic ladder operators of spin-orbital j respecting the anti-commutation relations $\{\hat{a}_i, \hat{a}_j^\dagger\} = \delta_{ij}$ and $\{\hat{a}_i, \hat{a}_j\} = \{\hat{a}_i^\dagger, \hat{a}_j^\dagger\} = 0$. Importantly, $\hat{H}_f(t)$ is controllable in the sense that any unitary matrix can be generated by solving its Schrödinger equation [48, 49].

We note that while the first term of $\hat{H}_f(t)$ is unphysical since it breaks the parity symmetry of fermions, the quadratic and quartic terms occur in many physical models. This makes $\hat{H}_f(t)$ attractive for designing driven physically inspired ansätze as we are guaranteed that drive terms of form $\alpha(t) \hat{a} + \alpha^*(t) \hat{a}^\dagger$ will not commute with the physical problem Hamiltonian. Interestingly, the use of such terms has been proposed in the context of variational error suppression [4] as they may allow a variational state to re-enter a particular symmetry sector to correct for the effect of symmetry-breaking errors.

In the QOCA variational form, we propose to first write $\hat{H}_f(t)$ keeping only the quadratic and quartic terms that also appear in \hat{H}_{prob} , along with few additional symmetry-breaking drive terms. As in Eq. (9), we then parametrize the resulting time-evolution-like operator using the associated $\alpha(t)$, $\beta(t)$, and $\gamma(t)$ coefficient as parameters. With these choices, the QOCA variational form generates circuits that are only slightly different from those generated by the problem Hamiltonian.

We also note that the principles of this analysis can be extended to the simulation of non-fermionic Hamiltonians, provided a controllable Hamiltonian for these systems.

III. QOCA FOR THE FERMİ-HUBBARD MODEL

For completeness, we start this section by reviewing the Fermi-Hubbard model and explain how we use the QOCA variational form to prepare its ground state. We motivate our choice of initial state, and elaborate on the selection and circuit decomposition of the drive terms. Finally, we introduce short-QOCA, a variant of QOCA that yields shorter circuits by dropping some terms of \hat{H}_{prob} from the Hamiltonian that generates the regular QOCA ansatz.

A. The Fermi-Hubbard model (FHM)

The Fermi-Hubbard model is an iconic model in the study of strongly correlated materials [50]. It describes interacting spin- $\frac{1}{2}$ fermions on a lattice where each site can be occupied by up to two particles of opposite spins. The Hamiltonian of the FHM for L lattice sites takes the form

$$\hat{H}_{\text{FHM}} = \underbrace{-t \sum_{\langle i,j \rangle, \sigma} \hat{a}_{i\sigma}^\dagger \hat{a}_{j\sigma}}_{\equiv \hat{T}} + \underbrace{U \sum_{i=1}^L \hat{n}_{i\uparrow} \hat{n}_{i\downarrow} - \mu \sum_{i,\sigma} \hat{n}_{i\sigma}}_{\equiv \hat{V}}, \quad (11)$$

where i, j are the lattice-site indices, and $\sigma = \{\uparrow, \downarrow\}$ labels the spin degree of freedom. In the first term, $\langle i, j \rangle$ denotes a sum over nearest-neighbor sites, and $\hat{n}_{i\sigma} = \hat{a}_{i\sigma}^\dagger \hat{a}_{i\sigma}$ is the occupation operator of the spin-orbital labeled $i\sigma$.

The first term of Eq. (11) represents hopping between neighboring sites with amplitude $-t$ and will generally be referred to as \hat{T} . This term is diagonal in momentum space if periodic boundary conditions are used, and its ground state consists of delocalized plane waves. The second term is a non-linear, on-site Coulomb repulsion of strength U , while the last term is the chemical potential. These last two terms are diagonal in the position basis and, taken together, are denoted \hat{V} . The ground state of \hat{V} is described by wave functions localized on the sites.

A particularly interesting instance of the FHM is the half-filling regime (which occurs for $\mu = U/2$) at intermediate coupling, $U/t \sim 4$. In this regime, both \hat{T} and \hat{V} contribute significantly to the system's energy, thus creating competition between the localized and delocalized states of the electrons, leading to rich physics such as the Mott transition. Because it becomes impossible to accurately treat either part of the Hamiltonian perturbatively, numerical exact diagonalization of the FHM is difficult beyond 24 lattice sites at half-filling [51]. As we seek to benchmark the usefulness of our variational form for all cases, we work in this particularly challenging regime.

Despite its apparent simplicity, this model has been used to study systems ranging from heavy fermions [52] to high-temperature superconductors [53, 54]. As a result, it is an interesting problem to benchmark near-term

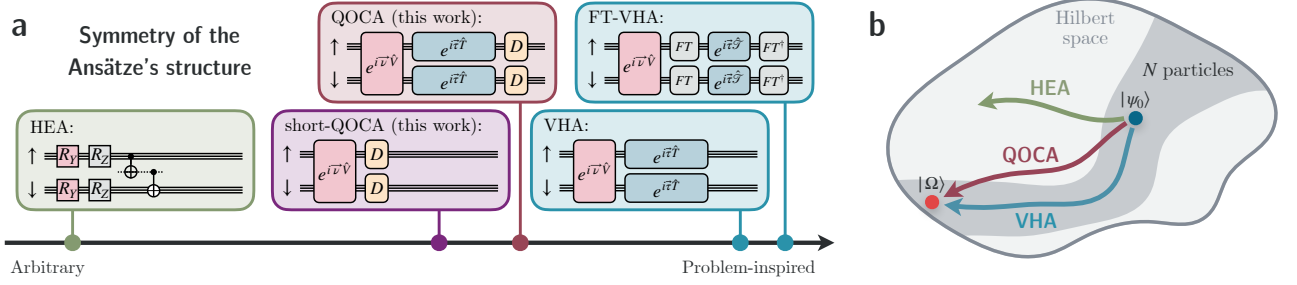


FIG. 1. **a** Single circuit layer of the ansätze studied in this work arranged by the symmetry of their structure. A high symmetry means that the ansatz is completely built around the problem Hamiltonian while a low one reflects the arbitrariness of its circuit. We show the hardware-efficient Ansatz (HEA) Eq. (2), the variational Hamiltonian Ansatz (VHA) Eq. (3), the Fourier-transformed VHA (FT-VHA) Eq. (4), the Quantum-Optimal-Control-inspired Ansatz (QOCA) Eq. (9) along with a shallower version of QOCA, the short-QOCA ansatz Eq. (18). The horizontal lines represent the qubit registers that encode the spin orbitals associated with the \uparrow or \downarrow spins. For HEA, the entangling block is a ladder of CNOT similar to the ones in the *Notation* box of Figure 2. For all other ansätze, \hat{T} and \hat{V} are respectively the kinetic and interaction parts of the problem Hamiltonian and $\{\tau, \nu\}$ are their associated variational parameters. For FT-VHA, we have that $\hat{T} = \text{FT} \hat{T} \text{FT}^\dagger$. The drive circuit D is defined in Eq. (17) and illustrated in Figure 2. **b** Possible paths in the Hilbert space for the HEA, VHA and QOCA variational forms. The initial state $|\psi_0\rangle$ and the target state $|\Omega\rangle$ are in the same symmetry sector containing N particles. Since HEA does not conserve the symmetries of \hat{H} , its path easily escapes from the fixed particle number subspace, while VHA is restricted to it. By introducing symmetry-breaking terms, QOCA has the ability to escape slightly from the N particles subspace to find shortcuts in Hilbert space.

quantum computers [55], and a useful performance test for variational ansätze. For these reasons, variational quantum algorithms have already been used to find the ground state of the FHM, for example using the HEA variational form [56], the VHA [21–23, 57, 58], and other symmetry-preserving ansätze [21, 25, 55, 59, 60].

B. Encoding and parametrization of the ansätze

We use the Jordan-Wigner (JW) transformation to encode fermionic Fock states into qubits registers, as detailed in Appendix A. Moreover, we work in real space and order the basis vectors for the $2L$ spin orbitals as $|f_{1\uparrow} \dots f_{L\uparrow}; f_{1\downarrow} \dots f_{L\downarrow}\rangle$ with $f_p \in \{0, 1\}$ the occupation of orbital p .

Using this purely conventional choice, in Fig. 1a we schematically draw one layer of the circuits implementing the different ansätze discussed above and arranged by the symmetry of their structure. A highly symmetric ansatz is completely built around \hat{H}_{prob} while a weakly symmetric construction is arbitrary with respect to the problem.

To parametrize these circuits, we consider two possible strategies: one corresponding to full parametrization of the single- and two-qubit gates and the other having a number of parameters that only grows with the depth of the ansatz, but not with the number of qubits. Whenever used, the latter is specified with the label ‘scalable’. Both strategies are elaborated on in Appendix B and details of the numerical simulation are presented in Appendix C.

C. Initial state

In general, the performance of VQAs strongly depends on the choice of initial state and variational parameters. The initial state acts as an educated guess to the target state and is often chosen such as to be easily computable classically. Moreover, because the initialization stage of a variational algorithm should be straightforward or otherwise be treated as a separate routine [61], we are interested in benchmarking the performance of the QOCA variational form for the simple initial state

$$|\psi_0\rangle = H^{\otimes N} |0\rangle = |+\rangle^{\otimes N}, \quad (12)$$

where H is the Hadamard gate. In addition to being easy to prepare, this initial state corresponds to half-filling and zero total spin, placing it in the same symmetry sector as the target state.

While this choice allows us to demonstrate the usefulness of the QOCA variational form given unstructured, simple initial conditions, we also show how the convergence can be improved further by using the ground state of the non-interacting FHM fixing $U = \mu = 0$ in Eq. (11) as initial state. More details on how to prepare this more complex state are provided in Appendix D.

D. Drive Hamiltonians

With the goal of reducing the number of variational parameters, we fix $\alpha_j(t)$ to 1 and i in Eq. (10) leading to

$$\hat{H}_1 = \sum_{j=1}^L (\hat{a}_j^\dagger + \hat{a}_j), \quad (13)$$

$$\hat{H}_2 = \sum_{j=1}^L i(\hat{a}_j^\dagger - \hat{a}_j). \quad (14)$$

We moreover obtain the drive equations for a spinless system and independently apply the resulting circuit to the two subspaces corresponding to the spin projections up and down for all sites. Performing the JW transformation on Eqs. (13) and (14), we find

$$\hat{H}_1 \mapsto \sum_{j=1}^L \hat{X}_j \bigotimes_{l < j} \hat{Z}_l, \quad (15)$$

$$\hat{H}_2 \mapsto \sum_{j=1}^L \hat{Y}_j \bigotimes_{l < j} \hat{Z}_l, \quad (16)$$

where \hat{X}, \hat{Y} and \hat{Z} are Pauli matrices. To incorporate these expressions into the QOCA variational form Eq. (9), we perform a first-order Trotter-Suzuki decomposition, arriving at the circuit equation for the d th layer of the ansatz,

$$\begin{aligned} & \prod_{k=1,2} e^{i\delta_{k,d} \hat{H}_k} \\ & \approx \prod_{j=1}^L \exp \left[i\delta_{1,d} \hat{X}_j \bigotimes_{l < j} \hat{Z}_l \right] \exp \left[i\delta_{2,d} \hat{Y}_j \bigotimes_{l < j} \hat{Z}_l \right], \end{aligned} \quad (17)$$

where $\{\delta_{k,d}\}$ are the variational parameters associated with the k th drive term of that layer. A schematic of the circuit implementing Eq. (17) for 4 qubits is illustrated in Fig. 2 where we also show a compiled version in terms of CNOTs.

E. The short-QOCA variational form

One drawback of QOCA is that, depending on the form of the drive, the corresponding quantum circuits can be long. Here we demonstrate a practical approach for the reduction of the circuit depth without compromising the performance.

Because the drive D in Fig. 2 and the kinetic part of the FHM Eq. (11) are both block-diagonal in the spin degree of freedom, we chose to remove the latter term, which is also costly in terms of two-qubit gates, arriving to the simplified form of the ansatz

$$\hat{U}_{\text{sqOCA}}(\boldsymbol{\nu}, \boldsymbol{\delta}) = \prod_d \left(\prod_j e^{i\nu_{j,d} \hat{V}_j} \prod_k e^{i\delta_{k,d} \hat{H}_k} \right), \quad (18)$$

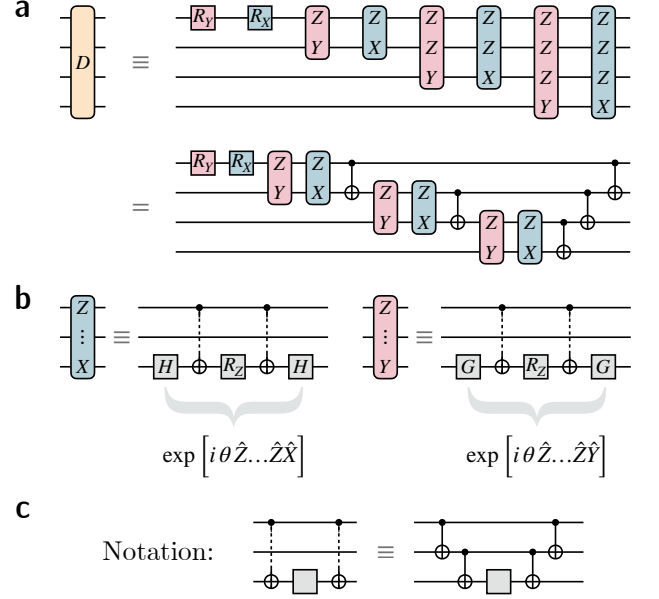


FIG. 2. **a** Circuit decomposition of the drive Eq. (17) used for QOCA. This circuit generalizes to any number of qubits by appending more $\hat{Z} \dots \hat{Z} \hat{Y}$ and $\hat{Z} \dots \hat{Z} \hat{X}$ multi-qubit gates at the end. We also show the circuit compiled to one- and two-qubit (CNOT) gates. **b** shows a decomposition of the multi-qubit gates based on a conventional approach to decompose exponentials of Pauli strings into circuits of CNOTs described in [62]. The transformation $H = (\hat{X} + \hat{Z})/\sqrt{2}$ is the Hadamard gate which changes between the \hat{X} and \hat{Z} bases and $G = (\hat{Y} + \hat{Z})/\sqrt{2}$ is the equivalent transformation between the \hat{Y} and \hat{Z} bases. The angles of the rotations $R_a(\theta) = \exp[-i\theta\hat{\sigma}_a/2]$ are the variational parameters, where $\hat{\sigma}_a$ is a Pauli matrix. **c** shows the notation shortcut used for the ladders of CNOTs.

where $\hat{V} = \sum_j \hat{V}_j$ is the on-site interaction part of the Fermi-Hubbard Hamiltonian Eq. (11) and $\boldsymbol{\nu} = \{\nu_{j,d}\}$ are the associated variational parameters. We refer to this simplified version of the QOCA variational form as *short-QOCA*, see Fig. 1.

IV. NUMERICAL RESULTS

In this section, we compare results obtained from numerical simulations of QOCA and short-QOCA for the Fermi-Hubbard model, and contrast these results with those obtained with the other ansätze discussed in this article. As an illustration of the use of QOCA beyond the Fermi-Hubbard model, we also present a comparison of the performance of this ansatz over a hardware-efficient approach and the UCCSD ansatz for a 12-qubit representation of the H_2O molecule.

Throughout this section, we use the fidelity with respect to the target state $|\Omega\rangle$ (i.e. ground state of the FHM or of the water molecule) as defined by

$$\text{Fidelity} = |\langle \psi(\boldsymbol{\theta}) | \Omega \rangle|^2, \quad (19)$$

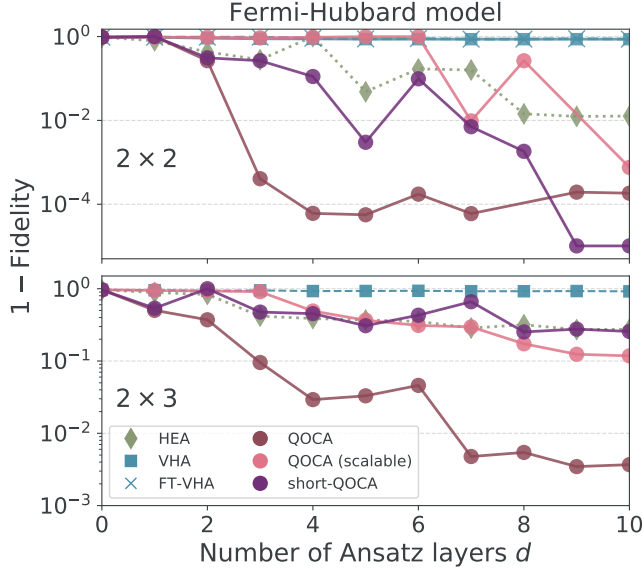


FIG. 3. Final variational state infidelities with respect to the target state as a function of the number of layers d of the variational forms of this work. Top panel is for a 2×2 plaquette while the bottom panel is a 2×3 system without periodic boundary conditions. The initial state is $|+\rangle^{\otimes N}$ for all cases. Data at $d = 0$ corresponds to the initial state alone, which has a fidelity of 0.035 with the target state. Unless specified, all ansätze are fully parametrized according to Appendix B 1.

to quantify the quality of the variational state $|\psi(\theta)\rangle$.

A. Fermi-Hubbard model

We consider 2×2 (8 qubits) and 2×3 (12 qubits) lattices of the Fermi-Hubbard model at half-filling with open boundary conditions. We note that the former configuration can also be seen as a periodic 1×4 chain. This allows us to compare with the FT-VHA variational form, as the fermionic Fourier transform on which this approach relies is defined for periodic boundary conditions. Importantly, we find that for smaller systems such as the four-qubits 2×1 dimer, all ansätze converge in a few tens of iterations on the ground-state energy with a precision of $< 10^{-7}$ using a single ansatz layer, $d = 1$, except for the HEA which requires two layers.

a. Comparing the ansätze For systems with four and six fermionic sites, we observe important variations in the ability of the different ansätze to converge to the ground state energy. This is illustrated in Fig. 3 which shows, for all ansätze, the final state infidelity as a function of the number of ansatz layers, d , initialized with the simple half-filled state of Eq. (12). The maximum fidelities achieved for all ansätze are reported in Table I along with resource counts using a circuit compilation in terms of CNOTs.

We first note that VHA and FT-VHA perform poorly for both system sizes and that their performance does

TABLE I. Maximum fidelities with respect to the ground state of the FHM, attained for d ansatz layers, each requiring a number n_θ/d of variational parameters and n_{CX}/d CNOTs per layer. The latter estimate assumes an all-to-all connectivity and the same compiling procedure is used for all ansätze.

	Hubbard model	Max Fid.	d	n_θ/d	n_{CX}/d
2×2 (8 qubits)	HEA	0.9876	9	16	7
	VHA	0.1343	8	8	56
	FT-VHA	0.1315	7	8	120
	QOCA	0.9999	4	16	88
	QOCA (scalable)	0.9992	10	5	88
	short-QOCA	0.9999	9	12	40
2×3 (12 qubits)	HEA	0.7276	10	24	11
	VHA	0.0804	10	13	116
	QOCA	0.9965	9	25	172
	QOCA (scalable)	0.8822	10	6	172
	short-QOCA	0.7476	8	18	68

not improve with the addition of more entangling layers, *i.e.* increasing d . Because these ansätze are particle-number conserving, this observation suggests that VHA and FT-VHA may not efficiently search over all states of fixed particle number in the variational landscape, as was originally proposed. Moreover, since FT-VHA performs similarly to VHA for the 2×2 system, we also conclude that alternating bases with the fermionic Fourier transform does not yield superior results for these lattice sizes.

Interestingly, QOCA systematically reaches the ground state of the Fermi-Hubbard model with significantly more accuracy than VHA for both system sizes, indicating that the additional symmetry-breaking terms help the convergence. This advantage persists even when drastically reducing the number of variational parameters from 16 to 5 per layer in the case of the scalable parametrization of QOCA, which converged with 0.9992 fidelity at $d = 10$ for the 2×2 system. The hardware-efficient approach also performs better than VHA, although it uses considerably more parameters than all other ansätze given it generally requires more layers to achieve similar performances. It is unclear how one might reduce that number to a favorable scaling.

Data obtained with the short-QOCA variational form show that the QOCA circuits can be substantially shortened by removing more than half of the two-qubit gates at every step without much compromise on the performance for small systems. In fact, for the 2×2 Hubbard model, a fidelity of 0.9999 is achieved with 9 layers of this ansatz.

With improved fidelities for shallower circuits which use fewer variational parameters than standard approaches, we find that QOCA provides significant gain with respect to other common ansätze.

b. The benefits of breaking symmetries Figure 4 shows the evolution of the average number of particles per lattice site (top panel) and the infidelity of the variational state with respect to the target state (bottom

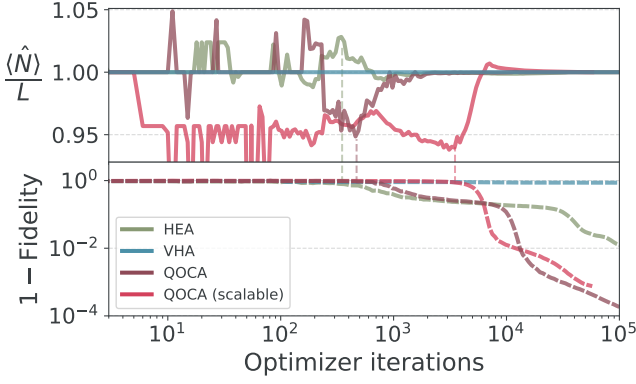


FIG. 4. Top: Average number of particles per lattice site in the variational state at every iteration of the VQA routine. $\langle \hat{N} \rangle = \sum_{i,\sigma} \langle \hat{n}_{i\sigma} \rangle$ is the total occupation and L is the number of sites. Bottom: corresponding variational state infidelity, $1 - |\langle \psi(\theta) | \Omega \rangle|^2$, with respect to the ground state of the Fermi-Hubbard model $|\Omega\rangle$. The results are for a 2×2 system and the initial state is $|+\rangle^{\otimes N}$ for all ansätze. Runs for ansatz depth $d = 9$ was used for HEA and $d = 10$ for the others, but this behavior is observed for most d .

panel) throughout the optimization process for the same simulations as in Fig. 3.

Focusing first on the top panel we first note that, because the initial state $|+\rangle^{\otimes N}$ is half-filled, all variational states begin in the correct particle-number symmetry sector of the Hilbert space with $\langle \hat{N} \rangle / L = 1$. Because VHA does not contain terms that allow the particle number to change, this quantity is observed to be constant throughout the optimization. We hypothesize that the poor performance of this ansatz in reaching the ground state is caused by the inability of this variational form to overcome local minima in parameter space.

In contrast, with their particle-non-conserving drive terms, both parametrizations of QOCA allow the average site occupancy to deviate from $\langle \hat{N} \rangle / L = 1$ as the drive angles are being tuned away from zero by the optimizer. As seen in Fig. 4, this can lead to the sharp features observed in the first few $\sim 10^2$ iterations as the classical optimizer can initially overweight the value of individual terms. Over the full optimization, the number of particles deviates only slightly from the target value $\langle \hat{N} \rangle / L = 1$ with changes of only $\sim 5\%$ of the site occupancy. This is an indication that the symmetry-breaking terms in QOCA allow the ansatz to explore a Hilbert space that is slightly larger than the manifold of fixed particle number. Nevertheless, we find that these relatively small excursions out of the target symmetry sector can significantly ease convergence of the VQA. Indeed, we observe that the onset of the return to the target symmetry sector, as indicated by the vertical dashed lines in Fig. 4 is often associated with the abrupt descents in the infidelity, which may indicate that regions of steep gradients in parameter space are found.

This behavior is also observed for the hardware-

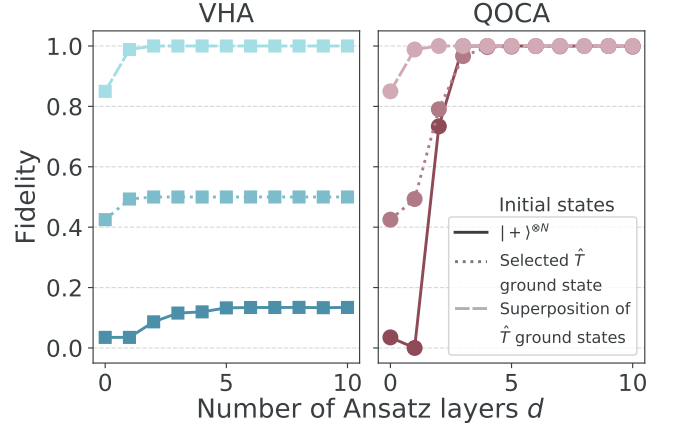


FIG. 5. Variational state fidelities with respect to the ground state of the 2×2 FHM as a function of the number of ansatz layers, d , for the VHA and QOCA variational forms. Results with three initial states are presented: (solid) Hadamard gates on every qubit $|+\rangle^{\otimes N}$, (dotted) a selected ground state of \hat{T} corresponding to $|\Omega_T^{(1)}\rangle$ of Appendix D, and (dashed) a superposition of ground states of \hat{T} corresponding to $|\Omega_T\rangle$ of Appendix D.

efficient ansatz of Eq. (2) which also, does not preserve the symmetries of \hat{H}_{prob} . This phenomenon is not particular to the realizations displayed in the figure, and it is also observed for other system sizes and initial states.

We note, however, that these desired regions in parameter space would never be found if an error-mitigation technique based on symmetry verification were employed [63, 64]. Indeed, in these schemes the variational states are post-selected after the energy measurements only if they conserve desired symmetries of the target state. However, other strategies for error mitigation remain applicable [65–67].

c. Initial state Because it provides a simple setting to benchmark the performance of the different ansätze, we have so far considered only the single easily-prepared initial state of Eq. (12). Improved approximation to the ground state can, however, be obtained if a more structured initial state is considered although at the price of more complex state preparation circuits.

In Fig. 5, we compare the performance of the VHA and QOCA variational forms on the 2×2 lattice with the following initial states of increasing complexity: i) the simple state $|+\rangle^{\otimes N}$, ii) one of the degenerate ground states of \hat{T} labelled $|\Omega_T^{(1)}\rangle$ in Appendix D, and iii) the superposition of ground states of \hat{T} labelled $|\Omega_T\rangle$ of Appendix D.

While the final variational state obtained with VHA strongly depends on the initial state, QOCA systematically achieves convergence with fidelity > 0.9999 , regardless of the initialization choice. Again because of its ability to move between symmetry sectors, these results illustrate QOCA’s robustness to simple, unstructured, initial conditions that can have very small overlaps with the tar-

TABLE II. Maximum fidelities obtained with d entangling layers, n_θ/d variational parameters and n_{CX}/d CNOTs per layer and different initial states for the QOCA, HEA and UCCSD variational forms applied to the water molecule. The initial states are either the Hartree-Fock (HF) approximation to the ground state or the equal superposition of all basis states $|+\rangle^{\otimes N}$. Again, the gate count estimate assumes an all-to-all connectivity and the same compiling procedure is used for all ansätze.

Water molecule (12 qubits)					
	Initial state	Max Fid.	d	n_θ/d	n_{CX}/d
QOCA	$ +\rangle^{\otimes N}$	0.9742	1	23	108
	$ +\rangle^{\otimes N}$	0.9931	5	23	108
	HF	0.9735	1	23	108
	HF	0.9917	7	23	108
HEA	$ +\rangle^{\otimes N}$	0.9820	8	24	11
UCCSD	HF	0.9748	1	8	528

get ground state. For the two variational forms, using a superposition of the degenerate ground states of \hat{T} as initial state (dashed lines) leads to convergence with fewer entangling layers. This, however, comes at the cost of significantly increasing the complexity of the initialization stage of the VQA (see Appendix D).

B. Proof-of-principle implementation of the H₂O molecule

The previous section illustrates how QOCA can approximate the ground state of the FHM with systematically more accuracy than other ansätze even when faced with unstructured initial conditions. In order to investigate the broader applicability of this method, we now benchmark the QOCA variational form on a quantum chemistry problem. As a proof-of-principle test, we consider the H₂O molecule in its equilibrium configuration. Because we freeze the core orbitals, this problem maps to 12 qubits using the STO3G basis set. The Hamiltonian is obtained using the PySCF driver as provided in Qiskit Chemistry [68]. We compare the performance of QOCA against HEA together with the well-known chemistry-inspired UCCSD ansatz [3]. Because the Hamiltonian describing the water molecule has significantly more terms than the FHM, directly implementing Hamiltonian-based ansätze as it is done above would lead to very long circuits. Therefore, we do not consider VHA for this problem.

In consequence, as a simple implementation of QOCA to a quantum chemistry problem, we use a variation of the ansatz based on the 12-qubit Hamiltonian of an open 1×6 Fermi-Hubbard chain with the drive terms of Eqs. (13) and (14). Although the water molecule Hamiltonian describes a richer set of fermionic interactions than the FHM, this choice of ansatz offers one of the simplest construction that simulates electron-electron correlations and is therefore a good starting point. More-

over, the ansatz is fully parametrized as before and the simulations were achieved under the same numerical conditions.

The maximum fidelities achieved for the QOCA, HEA and UCCSD variational forms are reported in Table II for different number of ansatz layers d and initial states, which are either the Hartree-Fock (HF) approximation to the ground state or the equal superposition of all basis states $|+\rangle^{\otimes N}$. Both initial states require one layer of single-qubit gates to prepare. The number of variational parameters (n_θ/d) and CNOT gates (n_{CX}/d) per layer are also presented. For the case of UCCSD we use $d = 1$, as it is proven to be enough for the simulation of chemical systems [26, 69]. For this reason, UCCSD uses significantly fewer parameters than other approaches, however, the resulting circuit requires roughly the same two-qubit-gate count as a $d = 5$ QOCA circuit.

We observe that a single layer ($d = 1$) QOCA circuit can prepare the ground state of the water molecule with fidelity 0.9742, a performance which is comparable to that of the well-established UCCSD ansatz (0.9748). However, while this does not improve the performance of UCCSD, adding layers up to $d = 5$ for QOCA increased the fidelity to 0.9931. Interestingly, the $|+\rangle^{\otimes N}$ initial state, which has a 9.95×10^{-5} overlap with the target state, yields better results for QOCA with fewer ansatz layers than the Hartree-Fock initial state, which has a 0.9735 overlap. These simulations suggest that QOCA can be useful also for quantum-chemistry problems. Modifying the QOCA circuit to better reproduce the interactions between the spin orbitals of the water molecule could lead to further improvements in performance.

V. CONCLUSION

We introduced the Quantum-Optimal-Control-inspired Ansatz by adding carefully chosen symmetry-breaking drive terms to the problem Hamiltonian and parametrizing the resulting time-evolution-like operator. We first applied QOCA to the half-filled Fermi-Hubbard model and found that in most cases it yields to a faster and more accurate convergence than standard approaches, even with unstructured initial states having little overlap with the target ground state. We showed evidence that this improved convergence is made possible by the symmetry-breaking terms allowing for small excursions outside of the target symmetry sector of the problem Hamiltonian. Moreover, we used QOCA to prepare the ground state of the water molecule, and showed that it can surpass the commonly used UCCSD ansatz with drastically shorter circuits.

Its broader applicability and the flexibility in choosing drive terms make QOCA a promising approach to tackle a wide range of quantum chemistry and materials problems on near-term quantum computers. Although the QOCA circuits are currently too deep to be imple-

mented reliably on today’s quantum devices, we expect that it may exhibit some resilience to symmetry-breaking errors. Our work represents a first step towards the development of a more general class of symmetry-breaking ansätze for variational quantum algorithms.

ACKNOWLEDGMENTS

We thank David Poulin, Jonathan Gross and Alexandre Daoust for useful discussions. This work was un-

dertaken thanks in part to funding from NSERC, the Canada First Research Excellence Fund and the U.S. Army Research Office Grant No. W911NF-18-1-0411.

Note added After completion of this work, we became aware of related work that was recently posted [70].

-
- [1] J. Preskill, Quantum computing in the nisq era and beyond, *Quantum* **2**, 79 (2018).
 - [2] K. Wright, K. Beck, S. Debnath, J. Amini, Y. Nam, N. Grzesiak, J.-S. Chen, N. Pienti, M. Chmielewski, C. Collins, *et al.*, Benchmarking an 11-qubit quantum computer, *Nature Communications* **10**, 1 (2019).
 - [3] A. Peruzzo, J. McClean, P. Shadbolt, M.-H. Yung, X.-Q. Zhou, P. J. Love, A. Aspuru-Guzik, and J. L. O’Brien, A variational eigenvalue solver on a photonic quantum processor, *Nature communications* **5**, 4213 (2014).
 - [4] J. R. McClean, J. Romero, R. Babbush, and A. Aspuru-Guzik, The theory of variational hybrid quantum-classical algorithms, *New Journal of Physics* **18**, 023023 (2016).
 - [5] C. Zoufal, A. Lucchi, and S. Woerner, Quantum generative adversarial networks for learning and loading random distributions, *arXiv preprint arXiv:1904.00043* (2019).
 - [6] C. Bravo-Prieto, R. LaRose, M. Cerezo, Y. Subasi, L. Cincio, and P. J. Coles, Variational quantum linear solver: A hybrid algorithm for linear systems, *arXiv preprint arXiv:1909.05820* (2019).
 - [7] M. Schuld and N. Killoran, Quantum machine learning in feature hilbert spaces, *Physical review letters* **122**, 040504 (2019).
 - [8] V. Havlíček, A. D. Córcoles, K. Temme, A. W. Harrow, A. Kandala, J. M. Chow, and J. M. Gambetta, Supervised learning with quantum-enhanced feature spaces, *Nature* **567**, 209 (2019).
 - [9] E. Farhi, J. Goldstone, and S. Gutmann, A quantum approximate optimization algorithm, *arXiv preprint arXiv:1411.4028* (2014).
 - [10] P. K. Barkoutsos, G. Nannicini, A. Robert, I. Tavernelli, and S. Woerner, Improving variational quantum optimization using cvar, *Quantum* **4**, 256 (2020).
 - [11] M. Reiher, N. Wiebe, K. M. Svore, D. Wecker, and M. Troyer, Elucidating reaction mechanisms on quantum computers, *Proceedings of the National Academy of Sciences* **114**, 7555 (2017).
 - [12] D. Wecker, M. B. Hastings, N. Wiebe, B. K. Clark, C. Nayak, and M. Troyer, Solving strongly correlated electron models on a quantum computer, *Physical Review A* **92**, 062318 (2015).
 - [13] J. Olson, Y. Cao, J. Romero, P. Johnson, P.-L. Dallaire-Demers, N. Sawaya, P. Narang, I. Kivlichan, M. Wasielewski, and A. Aspuru-Guzik, Quantum information and computation for chemistry, *arXiv preprint arXiv:1706.05413* (2017).
 - [14] Y. Cao, J. Romero, J. P. Olson, M. Degroote, P. D. Johnson, M. Kieferová, I. D. Kivlichan, T. Menke, B. Peropadre, N. P. Sawaya, *et al.*, Quantum chemistry in the age of quantum computing, *Chemical reviews* **119**, 10856 (2019).
 - [15] A. Robert, P. K. Barkoutsos, S. Woerner, and I. Tavernelli, Resource-efficient quantum algorithm for protein folding, *arXiv preprint arXiv:1908.02163* (2019).
 - [16] A. Di Paolo, P. K. Barkoutsos, I. Tavernelli, and A. Blais, Variational quantum simulation of ultrastrong light-matter coupling, *arXiv preprint arXiv:1909.08640* (2019).
 - [17] B. T. Gard, L. Zhu, G. S. Barron, N. J. Mayhall, S. E. Economou, and E. Barnes, Efficient symmetry-preserving state preparation circuits for the variational quantum eigensolver algorithm, *npj Quantum Information* **6**, 1 (2020).
 - [18] P. K. Barkoutsos, J. F. Gonthier, I. Sokolov, N. Moll, G. Salis, A. Fuhrer, M. Ganzhorn, D. J. Egger, M. Troyer, A. Mezzacapo, *et al.*, Quantum algorithms for electronic structure calculations: Particle-hole hamiltonian and optimized wave-function expansions, *Physical Review A* **98**, 022322 (2018).
 - [19] R. Sagastizabal, X. Bonet-Monroig, M. Singh, M. Rol, C. Bultink, X. Fu, C. Price, V. Ostroukh, N. Muthusubramanian, A. Bruno, *et al.*, Error mitigation by symmetry verification on a variational quantum eigensolver, *arXiv preprint arXiv:1902.11258* (2019).
 - [20] M. Ganzhorn, D. J. Egger, P. Barkoutsos, P. Ollitrault, G. Salis, N. Moll, M. Roth, A. Fuhrer, P. Mueller, S. Woerner, *et al.*, Gate-efficient simulation of molecular eigenstates on a quantum computer, *Physical Review Applied* **11**, 044092 (2019).
 - [21] C. Cade, L. Mineh, A. Montanaro, and S. Stanisic, Strategies for solving the fermi-hubbard model on near-term quantum computers, *arXiv preprint arXiv:1912.06007* (2019).
 - [22] A. Montanaro and S. Stanisic, Compressed variational quantum eigensolver for the fermi-hubbard model, *arXiv preprint arXiv:2006.01179* (2020).
 - [23] D. Wecker, M. B. Hastings, and M. Troyer, Progress towards practical quantum variational algorithms, *Physical Review A* **92**, 042303 (2015).
 - [24] A. Kandala, A. Mezzacapo, K. Temme, M. Takita, M. Brink, J. M. Chow, and J. M. Gambetta, Hardware-efficient variational quantum eigensolver for small molecules and quantum magnets, *Nature* **549**, 242

- (2017).
- [25] P.-L. Dallaire-Demers, J. Romero, L. Veis, S. Sim, and A. Aspuru-Guzik, Low-depth circuit ansatz for preparing correlated fermionic states on a quantum computer, *Quantum Science and Technology* **4**, 045005 (2019).
 - [26] J. Romero, R. Babbush, J. R. McClean, C. Hempel, P. J. Love, and A. Aspuru-Guzik, Strategies for quantum computing molecular energies using the unitary coupled cluster ansatz, *Quantum Science and Technology* **4**, 014008 (2018).
 - [27] I. D. Kivlichan, J. McClean, N. Wiebe, C. Gidney, A. Aspuru-Guzik, G. K.-L. Chan, and R. Babbush, Quantum simulation of electronic structure with linear depth and connectivity, *Physical review letters* **120**, 110501 (2018).
 - [28] A. J. Woitzik, P. K. Barkoutsos, F. Wudarski, A. Buchleitner, and I. Tavernelli, Entanglement production and convergence properties of the variational quantum eigensolver, *arXiv preprint arXiv:2003.12490* (2020).
 - [29] S. Sim, P. D. Johnson, and A. Aspuru-Guzik, Expressibility and entangling capability of parameterized quantum circuits for hybrid quantum-classical algorithms, *Advanced Quantum Technologies* **2**, 1900070 (2019).
 - [30] J. R. McClean, S. Boixo, V. N. Smelyanskiy, R. Babbush, and H. Neven, Barren plateaus in quantum neural network training landscapes, *Nature communications* **9**, 4812 (2018).
 - [31] F. Verstraete, J. I. Cirac, and J. I. Latorre, Quantum circuits for strongly correlated quantum systems, *Physical Review A* **79**, 032316 (2009).
 - [32] A. J. Ferris, Fourier transform for fermionic systems and the spectral tensor network, *Physical review letters* **113**, 010401 (2014).
 - [33] Z. Jiang, K. J. Sung, K. Kechedzhi, V. N. Smelyanskiy, and S. Boixo, Quantum algorithms to simulate many-body physics of correlated fermions, *Physical Review Applied* **9**, 044036 (2018).
 - [34] J. A. Fleck, J. Morris, and M. Feit, Time-dependent propagation of high energy laser beams through the atmosphere, *Applied physics* **10**, 129 (1976).
 - [35] M. Feit, J. Fleck Jr, and A. Steiger, Solution of the schrödinger equation by a spectral method, *Journal of Computational Physics* **47**, 412 (1982).
 - [36] R. Babbush, N. Wiebe, J. McClean, J. McClain, H. Neven, and G. K.-L. Chan, Low-depth quantum simulation of materials, *Physical Review X* **8**, 011044 (2018).
 - [37] D. Dong and I. R. Petersen, Quantum control theory and applications: a survey, *IET Control Theory & Applications* **4**, 2651 (2010).
 - [38] M. James, Quantum control theory (2014), *arXiv:1406.5260 [quant-ph]*.
 - [39] N. Khaneja, T. Reiss, C. Kehlet, T. Schulte-Herbrüggen, and S. J. Glaser, Optimal control of coupled spin dynamics: design of nmr pulse sequences by gradient ascent algorithms, *Journal of magnetic resonance* **172**, 296 (2005).
 - [40] F. Motzoi, J. M. Gambetta, S. Merkel, and F. Wilhelm, Optimal control methods for rapidly time-varying hamiltonians, *Physical Review A* **84**, 022307 (2011).
 - [41] D. d'Alessandro, *Introduction to quantum control and dynamics* (CRC press, 2007).
 - [42] S. A. Rice, Interfering for the good of a chemical reaction, *Nature* **409**, 422 (2001).
 - [43] M. Shapiro and P. Brumer, Quantum control of bound and continuum state dynamics, *Physics Reports* **425**, 195 (2006).
 - [44] N. Khaneja, T. Reiss, B. Luy, and S. J. Glaser, Optimal control of spin dynamics in the presence of relaxation, *Journal of Magnetic Resonance* **162**, 311 (2003).
 - [45] R. W. Heeres, P. Reinhold, N. Ofek, L. Frunzio, L. Jiang, M. H. Devoret, and R. J. Schoelkopf, Implementing a universal gate set on a logical qubit encoded in an oscillator, *Nature Communications* **8**, 94 (2017).
 - [46] H. R. Grimsley, S. E. Economou, E. Barnes, and N. J. Mayhall, Adapt-vqe: An exact variational algorithm for fermionic simulations on a quantum computer, *arXiv preprint arXiv:1812.11173* (2018).
 - [47] H. L. Tang, E. Barnes, H. R. Grimsley, N. J. Mayhall, and S. E. Economou, qubit-adapt-vqe: An adaptive algorithm for constructing hardware-efficient ansätze on a quantum processor, *arXiv preprint arXiv:1911.10205* (2019).
 - [48] G. Ortiz, J. E. Gubernatis, E. Knill, and R. Laflamme, Quantum algorithms for fermionic simulations, *Physical Review A* **64**, 022319 (2001).
 - [49] G. Ortiz, J. Gubernatis, E. Knill, and R. Laflamme, Erratum: Quantum algorithms for fermionic simulations [phys. rev. a 64, 022319 2001], *Physical Review A* **65**, 029902 (2002).
 - [50] J. Hubbard, Electron correlations in narrow energy bands, *Proceedings of the Royal Society of London. Series A. Mathematical and Physical Sciences* **276**, 238 (1963).
 - [51] S. Yamada, T. Imamura, and M. Machida, 16.447 tflops and 159-billion-dimensional exact-diagonalization for trapped fermion-hubbard model on the earth simulator, in *SC'05: Proceedings of the 2005 ACM/IEEE Conference on Supercomputing* (IEEE, 2005) pp. 44-44.
 - [52] K. Masuda and D. Yamamoto, Variational cluster approach to s-wave pairing in heavy-fermion superconductors, *Physical Review B* **91**, 104508 (2015).
 - [53] M. Guillot, *Compétition entre l'antiferromagnétisme et la supraconductivité dans le modèle de Hubbard appliqué aux cuprates* (Université de Sherbrooke., 2007).
 - [54] J. Kaczmarczyk, J. Spałek, T. Schickling, and J. Bünnemann, Superconductivity in the two-dimensional hubbard model: Gutzwiller wave function solution, *Physical Review B* **88**, 115127 (2013).
 - [55] P.-L. Dallaire-Demers, M. Stechly, J. F. Gonthier, N. T. Bashige, J. Romero, and Y. Cao, An application benchmark for fermionic quantum simulations, *arXiv preprint arXiv:2003.01862* (2020).
 - [56] M. Wilson, S. Stromswold, F. Wudarski, S. Hadfield, N. M. Tubman, and E. Rieffel, Optimizing quantum heuristics with meta-learning, *arXiv preprint arXiv:1908.03185* (2019).
 - [57] J.-M. Reiner, F. Wilhelm-Mauch, G. Schön, and M. Marthaler, Finding the ground state of the hubbard model by variational methods on a quantum computer with gate errors, *Quantum Science and Technology* **4**, 035005 (2019).
 - [58] G. Verdon, M. Broughton, J. R. McClean, K. J. Sung, R. Babbush, Z. Jiang, H. Neven, and M. Mohseni, Learning to learn with quantum neural networks via classical neural networks, *arXiv preprint arXiv:1907.05415* (2019).
 - [59] I. O. Sokolov, P. K. Barkoutsos, P. J. Ollitrault, D. Greenberg, J. Rice, M. Pistoia, and I. Taver-

- neli, Quantum orbital-optimized unitary coupled cluster methods in the strongly correlated regime: Can quantum algorithms outperform their classical equivalents?, *The Journal of Chemical Physics* **152**, 124107 (2020).
- [60] L. Xu, J. T. Lee, and J. Freericks, Test of the unitary coupled-cluster variational quantum eigensolver for a simple strongly correlated condensed-matter system, arXiv preprint arXiv:2001.06957 (2020).
- [61] S. Hadfield, Z. Wang, B. O’Gorman, E. G. Rieffel, D. Venturelli, and R. Biswas, From the quantum approximate optimization algorithm to a quantum alternating operator ansatz, *Algorithms* **12**, 34 (2019).
- [62] J. D. Whitfield, J. Biamonte, and A. Aspuru-Guzik, Simulation of electronic structure hamiltonians using quantum computers, *Molecular Physics* **109**, 735 (2011).
- [63] X. Bonet-Monroig, R. Sagastizabal, M. Singh, and T. O’Brien, Low-cost error mitigation by symmetry verification, *Physical Review A* **98**, 062339 (2018).
- [64] R. Sagastizabal, X. Bonet-Monroig, M. Singh, M. A. Rol, C. Bultink, X. Fu, C. Price, V. Ostroukh, N. Muthusubramanian, A. Bruno, *et al.*, Experimental error mitigation via symmetry verification in a variational quantum eigensolver, *Physical Review A* **100**, 010302 (2019).
- [65] K. Temme, S. Bravyi, and J. M. Gambetta, Error mitigation for short-depth quantum circuits, *Physical review letters* **119**, 180509 (2017).
- [66] S. Endo, S. C. Benjamin, and Y. Li, Practical quantum error mitigation for near-future applications, *Physical Review X* **8**, 031027 (2018).
- [67] A. Kandala, K. Temme, A. D. Corcoles, A. Mezzacapo, J. M. Chow, and J. M. Gambetta, Extending the computational reach of a noisy superconducting quantum processor, arXiv preprint arXiv:1805.04492 (2018).
- [68] Contributors, Qiskit: An open-source framework for quantum computing (2019).
- [69] P. J. O’Malley, R. Babbush, I. D. Kivlichan, J. Romero, J. R. McClean, R. Barends, J. Kelly, P. Roushan, A. Tranter, N. Ding, *et al.*, Scalable quantum simulation of molecular energies, *Physical Review X* **6**, 031007 (2016).
- [70] N. Vogt, S. Zanker, J.-M. Reiner, T. Eckl, A. Maruszczyk, and M. Marthaler, Preparing symmetry broken ground states with variational quantum algorithms, arXiv preprint arXiv:2007.01582 (2020).
- [71] M. J. Powell, A direct search optimization method that models the objective and constraint functions by linear interpolation, in *Advances in optimization and numerical analysis* (Springer, 1994) pp. 51–67.
- [72] M. J. Powell, Direct search algorithms for optimization calculations, *Acta numerica* **7**, 287 (1998).
- [73] M. J. Powell, A view of algorithms for optimization without derivatives, *Mathematics Today-Bulletin of the Institute of Mathematics and its Applications* **43**, 170 (2007).

Appendix A: Jordan-Wigner fermionic encoding

In the Jordan-Wigner transformation, each fermionic site is encoded into the state of two qubits with the mapping $(0, \uparrow, \downarrow, \uparrow\downarrow) \mapsto (00, 01, 10, 11)$. Moreover, the

fermionic ladder operators take the form

$$\begin{aligned}\hat{a}_p &\mapsto \hat{\sigma}_p \bigotimes_{l < p} \hat{Z}_l, \\ \hat{a}_p^\dagger &\mapsto \hat{\sigma}_p^\dagger \bigotimes_{l < p} \hat{Z}_l,\end{aligned}\quad (\text{A1})$$

where $\hat{\sigma} = |0\rangle\langle 1|$, \hat{Z} is the Pauli-Z operator and the indices denote the spin orbitals or qubits. For a lattice of L sites, we arrange the $N = 2L$ spin orbitals as $|f_{1\uparrow} \dots f_{L\uparrow}; f_{1\downarrow} \dots f_{L\downarrow}\rangle$ with $f_p \in \{0, 1\}$ the occupation of spin-orbital p .

With this mapping, hopping terms between spin-orbitals p and q with $p < q$ transform as

$$\hat{a}_p^\dagger \hat{a}_q + \hat{a}_q^\dagger \hat{a}_p \mapsto \frac{1}{2}(\hat{X}_p \hat{X}_q + \hat{Y}_p \hat{Y}_q) \bigotimes_{l=p+1}^{q-1} \hat{Z}_l, \quad (\text{A2})$$

where \hat{X} , \hat{Y} and \hat{Z} are Pauli matrices. The product of \hat{Z} operators, referred to as the JW string, vanishes when $q = p + 1$. Moreover, the number operator on spin-orbital p , and therefore the onsite Coulomb interaction between spin-orbitals p and q take the form

$$\begin{aligned}\hat{n}_p &= \hat{a}_p^\dagger \hat{a}_p \mapsto \frac{1}{2}(\hat{I} - \hat{Z}_p), \\ \hat{n}_p \hat{n}_q &\mapsto \frac{1}{4}(\hat{I} - \hat{Z}_p - \hat{Z}_q + \hat{Z}_p \hat{Z}_q).\end{aligned}\quad (\text{A3})$$

At half-filling, the single \hat{Z} s coming from the onsite interaction terms are canceled by similar terms arising from the chemical potential, leading to a simple expression for the potential

$$\hat{V} \mapsto \frac{U}{4} \sum_{i=1}^L \hat{Z}_{i\uparrow} \hat{Z}_{i\downarrow}, \quad (\text{A4})$$

which is diagonal in the computational basis.

Appendix B: Parametrization of the ansätze

1. Full parametrization

This strategy corresponds to taking all (or almost all) gate angles as variational parameters. This gives the classical optimizer enough freedom to explore the Hilbert space spanned by the ansatz at the cost of a longer optimization time. We note that the HEA has, by default, a *fully parametrized* configuration since all single-qubit gates are parametrized. Moreover, the same strategy for VHA consists of assigning one parameter to every $\hat{a}_{i\sigma}^\dagger \hat{a}_{j\sigma} + \text{h.c.}$ hopping terms and duplicating the parameter to take into account the two spin orientations. This is because at half-filling and zero total spin, there is a spin-inversion symmetry which removes the need to treat spins up and down differently. Additionally, every

term of the on-site interaction is associated with a variational parameter. The asymptotic scaling of number of variational parameters for all ansätze is summarized in Table III for both parametrization strategies.

2. Scalable parametrization

In a scalable parametrization strategy, we employ a number of variational parameters that is independent of the system size. Because there are fewer parameters, we expect the optimization to be faster, but larger circuit depths might be necessary to achieve the same accuracy as full parametrization.

Although it is less clear how one would achieve a scalable parametrization for hardware-efficient approaches, a simple strategy exists for physics-inspired ansätze such as QOCA. It consists in grouping the individual terms of the Hamiltonian into a constant number of sets containing commuting terms. For example, a common way of grouping the different terms of the FHM on a 2D lattice is

$$\hat{H}_{\text{FHM}} = \hat{H}_{h,\text{even}} + \hat{H}_{h,\text{odd}} + \hat{H}_{v,\text{even}} + \hat{H}_{v,\text{odd}} + \hat{H}_U, \quad (\text{B1})$$

where the first four terms now group the even and odd, vertical and horizontal hopping terms, while \hat{H}_U collects the on-site interaction terms. Note that for the 3D FHM, two additional sets of hopping terms covering the third dimension would be necessary.

	Full parametrization	Scalable parametrization
HEA	$2Ld$	–
VHA	$(\eta + 1)Ld$	$(2\eta + 1)d$
FT-VHA	$(\eta + 1)Ld$	$(\eta + 1)d$
QOCA	$(\eta + 3)Ld$	$(2\eta + 3)d$
sQOCA	$3Ld$	$3d$

TABLE III. Asymptotic scaling of the number of variational parameters of the ansätze of this work for the full and scalable parametrization strategies. These numbers are for periodic η -dimensional Fermi-Hubbard systems of L lattice sites. d is the number of layers of the ansätze.

Appendix C: Numerical simulations

All simulations are done using Qiskit Aqua’s VQA tools [68]. Because noise is not considered, a unitary statevector simulator is used. For simplicity, we also assumed all-to-all connectivity of the qubits, although this is not strictly needed. We chose the COBYLA [71–73] method as the classical optimizer with a maximum number of function evaluation of $\sim 10^5$. This number was justified as being reasonable in [21] using experimentally realistic arguments.

Whenever possible, we initialize all variational parameters to zero. With this choice, Hamiltonian-based ansätze implement the identity operator at the start of the optimization routine and the variational search begins from the initial state. In contrast to a random initialization of the parameters, this strategy also avoids the need of doing repeated VQA runs and post-selecting the best results. However, in the case of short-QOCA, this strategy results in premature convergence of the optimizer into states close to the initial guess, forcing us to use a random initialization of the parameters. Interestingly, even without post-selection, this did not hinder the convergence capability thanks to the robustness of QOCA regarding initial conditions.

Finally, all layers of the ansätze are optimized simultaneously. Further improvement can potentially be achieved by adopting a layer-by-layer optimization strategy as in Ref. [23].

For the simulation of the water molecule, we use the PySCF driver to obtain the Hamiltonian as provided

Appendix D: Initial states

In most quantum simulations of the FHM reported in the literature [21–23, 25, 57, 58, 60], the initial state is the ground state of the non-interacting FHM *i.e.* fixing $U = \mu = 0$ in Eq. (11). Because the resulting Hamiltonian is diagonal in Fourier space, this is a convenient choice because the ground state is readily computed classically. However, preparing this on a quantum computer generally requires very long quantum circuits as it involves the fermionic Fourier transformation. Current implementations of this transformation [31, 33, 36] are defined only for periodic systems, which limits this initial state’s applicability. To the best of our knowledge, no implementation of an open-boundary-conditions fermionic Fourier transformation has been developed to date. Furthermore, the ground state of the non-interacting FHM can be degenerate which makes it difficult to choose which one or superposition thereof to use. This challenge is often pointed out as an open problem [21, 60], since in most VQA realization, prior knowledge of the target state is used to find the initial state that maximizes the fidelity. It is unclear how one would make this choice as systems grow computationally intractable.

1. The non-interacting Fermi-Hubbard model

To see how this degeneracy arises, we consider the 1D non-interacting FHM ($U = \mu = 0$) with L sites and periodic boundary conditions. In momentum space, the Hamiltonian is given by a collection of free fermionic modes

$$\hat{\mathcal{T}} = \text{FT } \hat{T} \text{ FT}^\dagger = \sum_{k,\sigma=\{\uparrow,\downarrow\}} \varepsilon_k \hat{c}_{k\sigma}^\dagger \hat{c}_{k\sigma}, \quad (\text{D1})$$

where the energy spectrum is

$$\varepsilon_k = -2t \cos\left(\frac{2\pi k}{L}\right). \quad (\text{D2})$$

In the above Hamiltonian, $\hat{c}_{k\sigma}^\dagger$ and $\hat{c}_{k\sigma}$ are respectively the creation and annihilation fermionic operators of momentum k and spin σ . They are obtained from the real-space ladder operators $\hat{a}_{k\sigma}^\dagger$ and $\hat{a}_{k\sigma}$ and the fermionic Fourier transformation as

$$\hat{c}_{k\sigma}^\dagger = \text{FT } \hat{a}_{k\sigma}^\dagger \text{FT}^\dagger = \frac{1}{\sqrt{L}} \sum_{j=0}^{L-1} e^{-i\frac{2\pi k}{L}j} \hat{a}_{j\sigma}^\dagger, \quad (\text{D3})$$

$$\hat{c}_{k\sigma} = \text{FT } \hat{a}_{k\sigma} \text{FT}^\dagger = \frac{1}{\sqrt{L}} \sum_{j=0}^{L-1} e^{i\frac{2\pi k}{L}j} \hat{a}_{j\sigma}. \quad (\text{D4})$$

Because k can only take discrete values, one notices that a degeneracy appears when there are energy levels at $\varepsilon_k = 0$ since these levels could be occupied or empty without affecting the ground state energy. It is straightforward to see from Eq. (D2) that this can happen only when $L = 4l$, with l an integer. In this case, there are two values of k (corresponding to $k = l$ and $k = 3l$) which leads to $\varepsilon_k = 0$. The degeneracy is therefore $4^2 = 16$ since each momentum mode can be empty, occupied by a \uparrow or \downarrow spin, or both. In the half-filled symmetry sector, the degeneracy is reduced to $\binom{4}{2} = 6$. Note that in the case $L \neq 4l$, the ground state of the non-interacting FHM is not degenerate and is a simple basis state in momentum space.

As mentioned above, this occasional degeneracy makes it difficult to guess which basis state (or superposition thereof) is the best initial state to use in a VQA. Although, one can select states that respect certain desired properties such as particle number, total spin and total momentum.

Typically, the degeneracy at $L = 4l$ can be lifted by applying a small perturbative Coulomb interaction U . In this case, the ground state of the non-interacting FHM

becomes a superposition of basis states in Fourier space. One must apply the FT^\dagger in order to transform this initial state into real space for the VQA.

2. Choosing and preparing the initial states

In the case of $L = 4$ (or 2×2), we computed the fidelity of the 16 degenerate ground states of Eq. (D1) with respect to the target ground state and post-selected the ones leading to the highest fidelity. This strategy is, of course, not scalable and therefore it remains unclear how one would proceed in practice in the case where the fidelity with the target ground state cannot be computed beforehand.

In the present case, this strategy yields two ground states with a fidelity of ≈ 0.425 with respect to the ground state of the full model. Labeling the spin orbitals $|f_{1\uparrow} \dots f_{L\uparrow}; f_{1\downarrow} \dots f_{L\downarrow}\rangle$, these two states in real space are

$$|\Omega_T^{(1)}\rangle = \text{FT}^\dagger |1100; 1100\rangle, \quad (\text{D5})$$

$$|\Omega_T^{(2)}\rangle = \text{FT}^\dagger |1001; 1001\rangle. \quad (\text{D6})$$

Preparing these two states requires applying Pauli- X gates on selected qubits followed by the fermionic Fourier transformation, something which requires long quantum circuits [31, 33, 36].

Adding a small perturbation $U = 1 \times 10^{-5}t$, we find that the following superposition of $|\Omega_T^{(1)}\rangle$ and $|\Omega_T^{(2)}\rangle$ yields a significantly larger fidelity to the true ground state of ≈ 0.85 :

$$\begin{aligned} |\Omega_T\rangle &= \frac{|\Omega_T^{(1)}\rangle - |\Omega_T^{(2)}\rangle}{\sqrt{2}} \\ &= \text{FT}^\dagger \frac{|1100; 1100\rangle - |1001; 1001\rangle}{\sqrt{2}}. \end{aligned} \quad (\text{D7})$$

This, however, increases the complexity of the initial state preparation.